Chinese Journal of Natural Medicines

Morin enhances the renoprotective effects of Empagliflozin in diabetic kidney disease *via* targeting ATF6–DAPK1 signaling

Yi Lei, Chenlin Gao, Xin Zhao, Wei Huang, Chunxia Jiang, Qi Wu, Betty Yuen Kwan Law, Yong Xu

Citation: Yi Lei, Chenlin Gao, Xin Zhao, Wei Huang, Chunxia Jiang, Qi Wu, Betty Yuen Kwan Law, Yong Xu, Morin enhances the renoprotective effects of Empagliflozin in diabetic kidney disease *via* targeting ATF6–DAPK1 signaling, Chinese Journal of Natural Medicines, 2026, 24(6), 720–733. doi: 10.1016/S1875–5364(26)61187–9.

View online: https://doi.org/10.1016/S1875–5364(26)61187–9

Chinese Journal of Natural Medicines 24 (2026) 720-733

Contents lists available at ScienceDirect

Chinese Journal of Natural Medicines

journal homepage: www.cjnmcpu.com/

Original article

Morin enhances the renoprotective effects of Empagliflozin in diabetic kidney disease *via* targeting ATF6-DAPK1 signaling

Yi Lei[a,b,c,d], Chenlin Gao[b,c,d], Xin Zhao[d,e], Wei Huang[b,c,d], Chunxia Jiang[a,b,c,d], Qi Wu[a,c,d,f], Betty Yuen Kwan Law[a,*], Yong Xu[a,b,c,d,*]

[a] *State Key Laboratory of Quality Research in Chinese Medicine, Faculty of Chinese Medicine, Macau University of Science and Technology, Avenida Wai Long, Taipa, Macau,999078, China*

[b] *Department of Endocrinology and Metabolism, The Affiliated Hospital of Southwest Medical University, Luzhou 646000, China*

[c] *Metabolic Vascular Disease Key Laboratory of Sichuan Province, Luzhou 646000, China*

[d] *Sichuan Clinical Research Center for Nephropathy, Luzhou 646000, China*

[e] *Department of Urology, The Affiliated Hospital of Southwest Medical University, Luzhou 646000, China*

[f] *Department of Pathology, The Affiliated Hospital of Southwest Medical University, Luzhou 646000, China*

ARTICLE INFO

Article history:
Received 12 August 2025
Revised 21 January 2026
Accepted 12 February 2026
Available online 20 June 2026

Keywords:
Morin
Empagliflozin
DAPK1
Mitochondrial dysfunction
Diabetic kidney disease

ABSTRACT

Diabetic kidney disease (DKD) is a major complication of diabetes mellitus, driven by hyperglycemia-induced oxidative stress, ER stress, and mitochondrial apoptosis. This study examined the protective effects of Morin against hyperglycemia-induced renal tubular injury, alone or in combination with the SGLT2 inhibitor Empagliflozin, with emphasis on the ATF6-DAPK1 axis. HK2 cells were exposed to high glucose with or without Morin and/or Empagliflozin. Cellular stress, mitochondrial function, and apoptosis were assessed. Morin-DAPK1 binding was examined *via* molecular docking, surface plasmon resonance (SPR), and cell thermal shift assay (CETSA). *db/db* mice received vehicle, Empagliflozin, Morin, or their combination for 14 weeks, followed by renal histological, biochemical, and metabolic evaluations. Morin reduced ROS accumulation, ER stress (p-PERK, p-eIF2α, CHOP, cleaved ATF6), mitochondrial dysfunction, and apoptosis in HK2 cells. It suppressed *DAPK1* mRNA expression *via* ATF6 inhibition and directly bound DAPK1 (Kd = 1.61 μmol·L^{-1}), disrupting its interaction with pro-apoptotic BAK/BIK. Empagliflozin indirectly downregulated DAPK1 through ER stress relief. Combination therapy synergistically reduced oxidative stress, preserved mitochondrial membrane potential, and prevented apoptosis. In *db/db* mice, both compounds improved renal structure, lowered blood glucose, reduced UACR, and inhibited kidney stress markers, with greater improvements in the combination group, which also alleviated hepatic steatosis. Morin exhibits renoprotective effects against high glucose-induced cellular stress and diabetic kidney disease, at least partially *via* DAPK1 targeting. Co-administration with Empagliflozin enhances these effects, supporting its potential as an adjunct therapy for hyperglycemia-induced kidney injury.

1. Introduction

Diabetes mellitus (DM) is a pervasive metabolic disorder characterized by chronic hyperglycemia that affects millions of people worldwide [1]. A significant complication of diabetes is diabetic nephropathy, a primary contributor to end-stage renal disease [2]. Chronic hyperglycemia drives cellular stress mechanisms such as endoplasmic reticulum (ER) stress, oxidative stress, and mitochondrial dysfunction, which collectively contribute to renal cellular damage and apoptosis [3, 4]. Although current therapeutic approaches primarily focus on glycemic control and general anti-inflammatory strategies, there remains a critical need to identify novel molecular targets that directly regulate stress-induced apoptotic pathways in diabetic kidney disease (DKD).

Empagliflozin, a sodium–glucose cotransporter 2 (SGLT2) inhibitor, is a standard-of-care therapy for DKD because of its glucose-lowering and renoprotective properties [5, 6]. In addition to improving glycemic control, it confers modest anti-oxidative, anti-inflammatory, and anti-ER stress effects [7-10]. Given its established clinical role, Empagliflozin provides a relevant benchmark against which to evaluate novel therapeutic candidates and to explore potential additive effects.

Morin, a naturally occurring flavonoid, has garnered significant attention for its potent antioxidant and anti-inflammatory effects [11-13]. As a dietary supplement, Morin has demonstrated various pharmacological benefits, including hepatoprotective, cardioprotective, neuroprotective and renal protective effects [12, 14-16]. Mechanistically, Morin can alleviate ER stress by attenuating p-GRP78/PERK/ATF6 signaling [17, 18]. However, previous studies on Morin and related flavonoids have largely emphasized general antioxidative properties without elucidating specific molecular targets linking ER stress to mitochondrial apoptosis in DKD.

* Corresponding author.
E-mail addresses: yklaw@must.edu.mo (B. Law); xywyll@swmu.edu.cn (Y. Xu)

https://doi.org/10.1016/S1875-5364(26)61187-9

Our preliminary bioinformatic and target-docking analyses revealed that Empagliflozin and Morin share overlapping molecular targets relevant to oxidative stress and inflammation, yet they act on complementary signaling nodes. Importantly, we identified Death-Associated Protein Kinase 1 (DAPK1) as a direct physical binding partner of Morin. DAPK1 is a calcium/calmodulin-dependent serine/threonine kinase that integrates ER stress signals, particularly *via* ATF6 activation, to promote mitochondrial apoptosis [19-22]. Elevated DAPK1 activity has been implicated in diabetic complications [23, 24]; however, it remains an underexplored therapeutic target in DKD.

We therefore hypothesized that Morin, by inhibiting ATF6 activation and directly binding DAPK1 to disrupt its pro-apoptotic interactions, would provide significant renoprotection in DKD. Its addition to the standard therapy Empagliflozin could further enhance overall efficacy *via* complementary mechanisms. To test this hypothesis, we evaluated the protective effects and mechanistic basis of Morin alone and in combination with Empagliflozin in cellular and murine DKD models, with a focus on the ATF6–DAPK1–mitochondrial apoptosis axis.

2. Materials and methods

2.1. Cell culture

HK2 cells, a proximal tubular cell line derived from normal human kidney, were obtained from Procell (CL-0109; Wuhan, China) and cultured in DMEM (Gibco, 11965092) supplemented with 10% FBS (Gibco, 10270106) and 1% penicillin/streptomycin (Gibco, 15140122) at 37 °C with 5% CO_2. For DAPK1 overexpression, HK2 cells were infected with lentivirus generated from the pLenti-puro plasmid carrying the cDNA sequence of the human DAPK1 gene (NM_004938). An empty pLenti-puro vector served as the control. Lentivirus was produced using Lipofectamine 3000 (Thermo Fisher, L3000001) and packaging plasmids psPAX2 (Addgene, 12260) and pMD2.G (Addgene, 12259).

2.2. Treatment protocols

HK2 cells were seeded in 6-well or 96-well plates (Corning, 3516) at a density of 1×10^4 cells/cm^2. After reaching 70%–80% confluence, cells were cultured in growth medium containing normal glucose (NG, 5.5 mmol·L^{-1}) or high glucose (HG, 33 mmol·L^{-1}; prepared with D-glucose, Sigma-Aldrich, G7021), either alone or in combination with Empagliflozin (10 μmol·L^{-1}; Selleckchem, S8022), Morin (50 μmol·L^{-1}; Selleckchem, S9110) and/or TC-DAPK 6 (a potent DAPK1/3 inhibitor, 100 nmol·mL^{-1}; MCE, HY-15513) for 48 h. All treatments were diluted in serum-free DMEM. Doses used for *in vitro* experiments were based on previous publications (Morin [13, 25] and Empagliflozin [26]) and our own preliminary dose-optimization (Supplementary Figure 1). TC-DAPK 6 [27] has IC_{50} of 69 and 225 nmol·mL^{-1} against DAPK1 and DAPK3. Therefore, 100 nmol·mL^{-1} was used for cell treatment.

2.3. Cell viability assay

Cell viability was assessed using the Cell Counting Kit-8 (CCK-8; Beyotime, C0037). After treatment, 10 μl of CCK-8 reagent was added to each well of a 96-well plate and incubated for 2 h at 37 °C. Absorbance was measured at 450 nm using a BioTek Synergy H1 microplate reader (BioTek Instruments, Winooski, VT, USA).

2.4. Measurement of reactive oxygen species (ROS)

Intracellular ROS levels were measured using 2',7'-dichlorodihydrofluorescein diacetate (DCFH-DA; Beyotime, S0033). Treated HK2 cells were incubated with 20 μmol·L^{-1} DCFH-DA in serum-free medium for 30 min at 37 °C. After washing with PBS, fluorescence intensity was measured at excitation/emission wavelengths of 485/535 nm using the BioTek Synergy H1 microplate reader. Mitochondrial superoxide production was determined using MitoSOX Red (Beyotime, S0061S) (5 μmol·L^{-1}, 10 min, 37 °C), followed by flow cytometry.

2.5. JC-1 and tetramethylrhodamine methyl ester (TMRM) staining for mitochondrial membrane potential

Mitochondrial membrane potential was assessed using the MitoProbe JC-1 Assay Kit (Thermo Fisher Scientific, M34152). Treated HK2 cells in 6-well plates (Corning, 3516) were incubated with 5 μmol·L^{-1} JC-1 dye (prepared in 1 mL serum-free medium per well) for 30 min at 37 °C in the dark. Cells were washed twice with 1 × PBS (Gibco, 10010023) and immediately analyzed using a fluorescence microscope (Nikon Eclipse Ti2, Japan). JC-1 aggregates (red fluorescence: excitation/emission 560/595 nm) and monomers (green fluorescence: excitation/emission 485/535 nm) were imaged. The fluorescence ratio of aggregates to monomers was calculated to determine mitochondrial health. Mitochondrial membrane potential was additionally quantified using tetramethylrhodamine methyl ester (TMRM; Invitrogen, T668) staining. Fluorescence intensity was measured by flow cytometry (BD FACSCanto II, BD Biosciences, USA) at excitation 548 nm and emission 574 nm.

2.6. Flow cytometry for apoptosis detection

Apoptosis was quantified using the Annexin V-PE/7-AAD Apoptosis Detection Kit (Yeasen Biotech, 40310ES50). After treatment, HK2 cells were trypsinized with 0.25% Trypsin-EDTA (Gibco, 25200056), neutralized with complete medium, and centrifuged at 300 × g for 5 min. Cells were washed twice in 1 × PBS and resuspended in 100 μL binding buffer (provided in the kit) at a density of 1×10^6 cells/mL. Cells were stained with 5 μL Annexin V-PE and 5 μL 7-AAD per sample for 15 min at room temperature in the dark. Stained cells were analyzed within 1 h using a BD FACSCanto II flow cytometer (BD Biosciences, USA). Quadrants Q2-4 and Q2-2 represent early and late apoptotic cells, respectively. Only early apoptotic cells were quantified.

2.7. Western blot analysis

Treated HK2 cells were lysed in RIPA buffer (Thermo Fisher Scientific, 89900) supplemented with 1 × protease inhibitor cocktail (Roche, 11697498001) and 1 × phosphatase inhibitor cocktail (Sigma-Aldrich, P0044). Mitochondrial and cytosolic fractions were isolated using the Mitochondria Isolation Kit for Cultured Cells (Thermo Fisher Scientific, 89874) as previously described [28]. Protein concentrations were quantified using the BCA Protein Assay Kit (Thermo Fisher Scientific, 23225). Equal amounts of protein (30 μg per lane) were separated by SDS-PAGE (4%–20% gradient gels; Bio-Rad, 4561094) and transferred to PVDF membranes (Millipore, IPVH00010). Membranes were blocked for 1 h in 5% non-fat milk (Bio-Rad, 1706404) in TBS-T (Tris-buffered saline with 0.1% Tween-20) and incubated overnight at 4 °C with the following primary antibodies against: cleaved PARP (1 ∶ 1000, #9541, CST), cleaved caspase-3 (1 ∶ 1000, #9664, CST), Bax (1 ∶ 5000, 60267-1-Ig, Proteintech), Bcl2 (1 ∶ 2000, 12789-1-AP, Proteintech), GRP78 (1 ∶ 2000, 11587-1-AP, Proteintech), p-PERK (1 ∶ 1000, #3179, CST), PERK (1 ∶ 1000, #3192, CST), p-eIF2α (1 ∶ 1000, #3398, CST), eIF2α (1 ∶ 1000, #9722, CST), CHOP (1 ∶ 2000, 15204-1-AP, Proteintech), ATF6 (1 ∶ 1000, NBP1-40256, Novus Biologicals), Mfn1 (1 ∶

2000, 66776-1-Ig, Proteintech), Mfn2 (1 ∶ 2000, 12186-1-AP, Proteintech), Fis1 (1 ∶ 2000, 10956-1-AP, Proteintech), Cytochrome C (CytoC; 1 ∶ 2000, 10993-1-AP, Proteintech), COX IV (1 ∶ 5000, 11242-1-AP, Proteintech), anti-DAPK1 (1 ∶ 2000, 25136-1-AP) and β-actin (1 ∶ 5000, 20536-1-AP, Proteintech). After washing with TBS-T, membranes were incubated with HRP-conjugated anti-rabbit IgG (1 ∶ 5000, #7074, CST) or anti-mouse IgG (1 : 5000, #7076, CST) secondary antibodies for 1 h at room temperature. Protein bands were visualized using the SuperSignal West Pico ECL Substrate (Thermo Fisher Scientific, 34577) and quantified using ImageJ software (v1.53).

2.8. Immunofluorescence staining

After treatment, cells were washed twice with 1 × PBS, fixed with 4% paraformaldehyde (PFA) for 15 min at room temperature, and permeabilized with 0.1% Triton X-100 (Sigma-Aldrich, T8787) in PBS for 10 min. Cells were blocked with 5% bovine serum albumin (BSA; Sigma-Aldrich, A7906) in PBS for 1 h and incubated overnight at 4 °C with anti-ATF6 antibody (1 : 250, NBP1-40256, Novus Biologicals). After washing, cells were incubated with Alexa Fluor 488-conjugated goat anti-rabbit IgG (1 : 1000, #A-11008, Invitrogen) for 1 h at room temperature in the dark.

For dual-labeling of CytoC and Tomm20, cells were co-stained with mouse anti-Tomm20 (1 ∶ 250, 66777-1-Ig, Proteintech) and rabbit anti-CytoC (1 ∶ 250, 10993-1-AP, Proteintech) antibodies overnight at 4 °C, followed by Alexa Fluor 488-conjugated anti-mouse IgG (1 ∶ 1000, #A-11001, Invitrogen) and Alexa Fluor 594-conjugated anti-rabbit IgG (1 ∶ 1000, #A-11012, Invitrogen). Nuclei were stained with Hoechst 33342 (5 μg·mL^{-1}, Beyotime, C1022) for 10 min. Images were captured using an Olympus FV2000 confocal microscope (Tokyo, Japan). For quantification of ATF6 nuclear localization, images were analyzed using ImageJ software (v1.53) by defining regions of interest (ROIs) corresponding to nuclei and to total cell area. Mean fluorescence intensity (MFI) of ATF6 within the nuclear ROIs was divided by MFI of total cell ATF6 to yield the nuclear/total ATF6 ratio for each cell.

2.9. Mitochondrial fragmentation index

For live-cell imaging, HK2 cells were incubated with Mito-Tracker Green FM (50 nmol·L^{-1}, Beyotime, C1048) in serum-free medium at 37 °C for 30 min. Cells were washed with pre-warmed PBS and stained with Hoechst 33342 (5 μg·mL^{-1}, Beyotime, C1022) for 10 min. Mitochondrial morphology was visualized using the Olympus FV2000 confocal microscope. Mitochondrial fragmentation was quantified blindly by two independent technicians. Fission events (punctate or fragmented mitochondria) were counted and expressed as a percentage of total mitochondria using the equation: (fission events/total mitochondria) × 100, where total mitochondria include fission, intermediate, and fusion types.

2.10. Measurement of mitochondrial superoxide production

Mitochondrial superoxide production was assessed using the MitoSOX™ Red Mitochondrial Superoxide Indicator (Yeasen Biotech, 40778ES50). Treated HK2 cells were incubated with 5 μmol·L^{-1} MitoSOX Red reagent (diluted in serum-free DMEM) for 10 min at 37 °C in the dark. Cells were washed twice with 1 × PBS, and fluorescence intensity was measured using a BioTek Synergy H1 microplate reader (BioTek Instruments) at excitation/emission wavelengths of 510/580 nm.

2.11. Target prediction and molecular docking

SwissTargetPrediction (http://swisstargetprediction.ch/) [29] was applied to predict the potential targets of Morin and Empagliflozin. The docking model between Morin and DAPK1 was calculated using CB-DOCK (http://clab.labshare.cn/cb-dock/php/) [30]. The crystal structure of DAPK1 (https://doi.org/10.2210/pdb8IE8/pdb) [31] was used for docking.

2.12. RT-qPCR analysis

Total RNA was isolated from HK2 cells using the RNeasy Mini Kit (Qiagen, 74104) following the manufacturer's protocol, including lysis with 350 μL Buffer RLT (provided in the kit).RNA concentration was quantified using a NanoDrop 2000 spectrophotometer (Thermo Fisher Scientific). One microgram of total RNA was reverse-transcribed into cDNA using the iScript™ cDNA Synthesis Kit (Bio-Rad, 1708890) in a 20 μL reaction volume. Quantitative PCR was performed with SsoAdvanced Universal SYBR Green Supermix (Bio-Rad, 1725271) using 0.5 μmol·L^{-1} of each primer (final concentration) in a 10 μL reaction volume. Reactions were run on a CFX96 Touch Real-Time PCR Detection System (Bio-Rad, 1855195) under the following conditions:

Initial denaturation: 95 °C for 3 min; 40 cycles: 95 °C for 10 s, 60 °C for 30 s.

Primer used were as follows:

DAPK1: forward 5'-CCAGACTGTCTTCCACCAACTC-3', reverse 5'-TCCTCACACTCACGTTCTCGCA-3'.

GAPDH: forward 5'-GTCTCCTCTGACTTCAACAGCG-3', reverse 5'-ACCACCCTGTTGCTGTAGCCAA-3'. The relative gene expression was calculated using the $2^{-\Delta\Delta Ct}$ method.

2.13. Surface plasmon resonance (SPR) analysis

Binding affinity studies were performed using a Biacore T200 instrument (Cytiva). Recombinant DAPK1 protein (Sino Biological, D01-11G) was immobilized onto a CM5 sensor chip (Cytiva, BR100012) using amine coupling chemistry. Morin (Sigma-Aldrich, M4008) was dissolved in DMSO and diluted in HBS-EP + buffer (10 mmol·L^{-1} HEPES, 150 mmol·L^{-1} NaCl, 3 mmol·L^{-1} EDTA, 0.05% *V/V* surfactant P20, pH 7.4; Cytiva, BR100669) to final concentrations of 1.56, 3.13, 6.25, 12.5, 25, and 50 μmol·L^{-1}. Empagliflozin (MedChemExpress, HY-15412) served as a control. Injections were performed in multi-cycle kinetic mode with a contact time of 120 s, a dissociation time of 180 s, and a baseline stabilization time of 30 s. The association and dissociation phases were measured, and the data were analyzed using Biacore T200 Evaluation Software employing a 1 : 1 binding model to determine the dissociation constant (K_d).

2.14. Cellular Thermal Shift Assay (CETSA)

HK2 cells were treated with Morin (50 μmol·L^{-1}; Sigma-Aldrich, Cat# M4008) or Empagliflozin (10 μmol·L^{-1}; MedChemExpress, Cat# HY-15412) for 48 h. After treatment, cells were collected and washed once with ice-cold PBS containing protease inhibitors (Roche, 11697498001).

Cells were counted and resuspended in PBS to a final density of 2 × 10^7 cells/mL. The cell suspension was aliquoted into PCR tubes (Axygen, Cat# PCR-02-C) and heated at the indicated temperatures (40, 45, 50, 55, 60, and 65 °C) for 3 min using a thermal cycler (Bio-Rad, T100). After heating, samples were cooled to room temperature.

Cells were then resuspended in NP-40 lysis buffer (Beyotime, Cat# P0013F) and subjected to three freeze–thaw cycles using liquid nitrogen. Lysates were centrifuged at 20 000 × g for 20 min at 4 °C, and the supernatants were collected. An equal volume of 2 × SDS loading buffer (Beyotime, Cat# P0015L) was added to each supernatant, followed by boiling at 100 °C for 10 min to denature proteins. A 30 μL aliquot of each sample was loaded onto SDS-PAGE gels for Western blot analysis as described above.

2.15. Co-Immunoprecipitation (Co-IP)

HK2 cell lysates (prepared in NP-40 lysis buffer with Roche protease inhibitors) were incubated with 5 μg anti-DAPK1 antibody (Proteintech, 67815-1-Ig) or control IgG (Proteintech, AC005) overnight at 4 °C. Protein A/G Magnetic Beads (Thermo Fisher, 88802) were added (20 μL per sample) and incubated for 2 h at 4 °C. Beads were washed 3 × with lysis buffer, and bound proteins were eluted in 2 × Laemmli buffer (Bio-Rad, 1610747). Western blot was performed using the following antibodies: DAPK1 (1 : 2000, Proteintech, 25136-1-AP); BAK (1 : 2000, Proteintech, 29552-1-AP) and BIK (1 : 1000, Cell Signaling Technology, #4592).

2.16. Animal models and treatment

Five-week-old male *db/m* and *db/db* mice were obtained from Huachuang Sino (Jiangsu, China) and housed under standard conditions with a 12-h light/dark cycle. All animal experiments were conducted according to the guidelines approved by the Experimental Animal Ethics Committee of Southwest Medical University, China (approval No. 20240725-001). Mice were acclimated for one week before the start of the experiment. The *db/m* mice (n = 6) were fed a normal diet for 14 weeks after one week of acclimation. The *db/db* mice (n = 8 per group) were divided into the following treatment groups: Vehicle (control); Empagliflozin (10 mg·kg^{-1} body weight/day, administered intragastrically, i.g.); low-dose Morin (50 mg·kg^{-1} body weight/day, i.g.); high-dose Morin (100 mg·kg^{-1} body weight/day, i.g.); combination of Empagliflozin (10 mg·kg^{-1}) and high-dose Morin (100 mg·kg^{-1}). The weight of the animals was recorded weekly. The doses of Empagliflozin and Morin for animal studies followed previous publications [13,32].

Blood glucose levels were measured at 6, 10, 12, 14, 16, 18, and 20 weeks after the start of treatment. For each measurement, approximately 20 μL of blood was collected from the tail vein using a sterile scalpel blade after cleaning the tail with 70% ethanol. Mice were gently restrained, and the distal tail was nicked to obtain a drop of blood, which was immediately analyzed using a glucometer (ACCU-CHEK, Roche Diagnostics). Hemostasis was achieved by applying gentle pressure to the tail after sampling.

At the end of the experiments, mice were euthanized by gradual-fill carbon dioxide (CO_2) inhalation at a flow rate of 20%–30% chamber volume per minute. After loss of consciousness, cervical dislocation was performed to ensure death, in accordance with institutional and national animal care guidelines. Kidneys and colons were collected and prepared for hematoxylin and eosin (H&E), periodic acid–Schiff (PAS), and Masson's trichrome staining. Urine samples were collected from each mouse at 6, 10, 15, and 20 weeks. Urinary albumin and creatinine concentrations were measured using a cobas 6500 urine analyzer series (Roche). The urinary albumin-to-creatinine ratio (UACR) was calculated to assess kidney function.

2.17. Statistical analysis

All data are presented as mean ± standard deviation (SD) (n = 3, 5, 6 or 8, as indicated). All statistical analyses were performed using GraphPad Prism 10.6 software (GraphPad Software, La Jolla, CA, USA). Prior to parametric testing, the normality of data distribution was assessed using the Shapiro–Wilk test, and homogeneity of variances was verified using Levene's test. All datasets included in this study met the assumptions of parametric tests. Potential outliers were identified using the Grubbs' test (alpha = 0.05) and excluded from the analysis if detected, with no more than one outlier removed per experimental group. For comparisons between two experimental groups, unpaired two-tailed Student's t-test was applied. For comparisons across three or more independent groups, one-way analysis of variance (ANOVA) followed by Tukey's post-hoc test for multiple pairwise comparisons was used. For longitudinal measurements such as body weight and blood glucose over time, repeated-measures two-way ANOVA was adopted to evaluate the effects of treatment and time. A P value of < 0.05 was considered statistically significant.

3. Results

3.1. Morin alleviates high-glucose-induced intracellular ROS production and apoptosis of proximal tubular cells

To determine the optimal concentrations of Morin and Empagliflozin for subsequent experiments, we first performed dose-optimization studies in HK2 cells under normal-glucose and high-glucose conditions (Supplementary Fig. 1). Morin (10–200 μmol·L^{-1}) (Supplementary Fig. 1A) and Empagliflozin (1–20 μmol·L^{-1}) (Supplementary Fig. 1B) were tested for their effects on cell viability. Both compounds showed dose-dependent protective effects against high-glucose (HG, 33 mmol·L^{-1})-induced cytotoxicity, with 50 μmol·L^{-1} Morin and 10 μmol·L^{-1} Empagliflozin providing maximal protection without affecting cell viability under normal-glucose (NG, 5.5 mmol·L^{-1}) conditions. These concentrations were therefore selected for all subsequent *in vitro* assays.

Under HG exposure, Empagliflozin or Morin alone partially prevented the decrease in cell viability, whereas their combination exerted a synergistic protective effect, significantly improving viability compared with either treatment alone (Fig. 1A). We then measured intracellular reactive oxygen species (ROS) levels using DCFDA fluorescence in each group (Fig. 1B). High-glucose treatment significantly increased ROS production to 189.6% ± 9.81% of the normal-glucose control. Treatment with Empagliflozin or Morin alone significantly reduced ROS levels to 152.0% ± 8.97% and 162.2% ± 6.87%, respectively. The combination treatment further decreased ROS production to 126.6% ± 6.15%, indicating a synergistic effect (Fig. 1B).

Excessive ROS generation is typically associated with dysregulated mitochondrial function. Therefore, we monitored changes in mitochondrial membrane potential using JC-1 staining. High-glucose treatment led to mitochondrial depolarization, as indicated by a decrease in red fluorescence (JC-1 aggregates) and an increase in green fluorescence (JC-1 monomers) (Figs. 1C and 1E). The combination treatment with Empagliflozin and Morin resulted in greater recovery of the aggregates-to-monomers ratio (Figs. 1C and 1E). To quantify cellular apoptosis, we performed flow cytometry using Annexin V-PE and 7-AAD staining. High-glucose treatment significantly increased the percentage of early apoptotic cells to 14.13% ± 0.55% (Figs. 1D and 1F). Empagliflozin and Morin each reduced the percentage of apoptotic cells to 9.20% ± 0.40% and 10.73% ± 0.45%, respectively. The combination treatment showed a synergistic effect on suppressing apoptosis, reducing it to 5.13% ± 0.40% (Figs. 1D and 1F). We then examined the expression of apoptotic markers, including cleaved PARP, cleaved caspase-3, Bax, and Bcl2, in each treatment group (Fig. 1G). High-glucose treatment increased the levels of cleaved PARP and cleaved caspase-3 as well as the pro-apoptotic protein Bax, whereas it decreased the anti-apoptotic protein Bcl2. Treatment with Empagliflozin or Morin individually modulated these markers in favor of cell survival (Fig. 1G). Their combination showed a synergistic effect that enhanced the protective protein expression profile (Fig. 1G). In summary, these results demonstrate that Morin exhibits protective effects against high-glucose-induced ROS production and apoptosis in HK2 cells. The combination with Empagliflozin yielded better protective outcomes, suggesting a synergistic effect under hyperglycemic conditions.

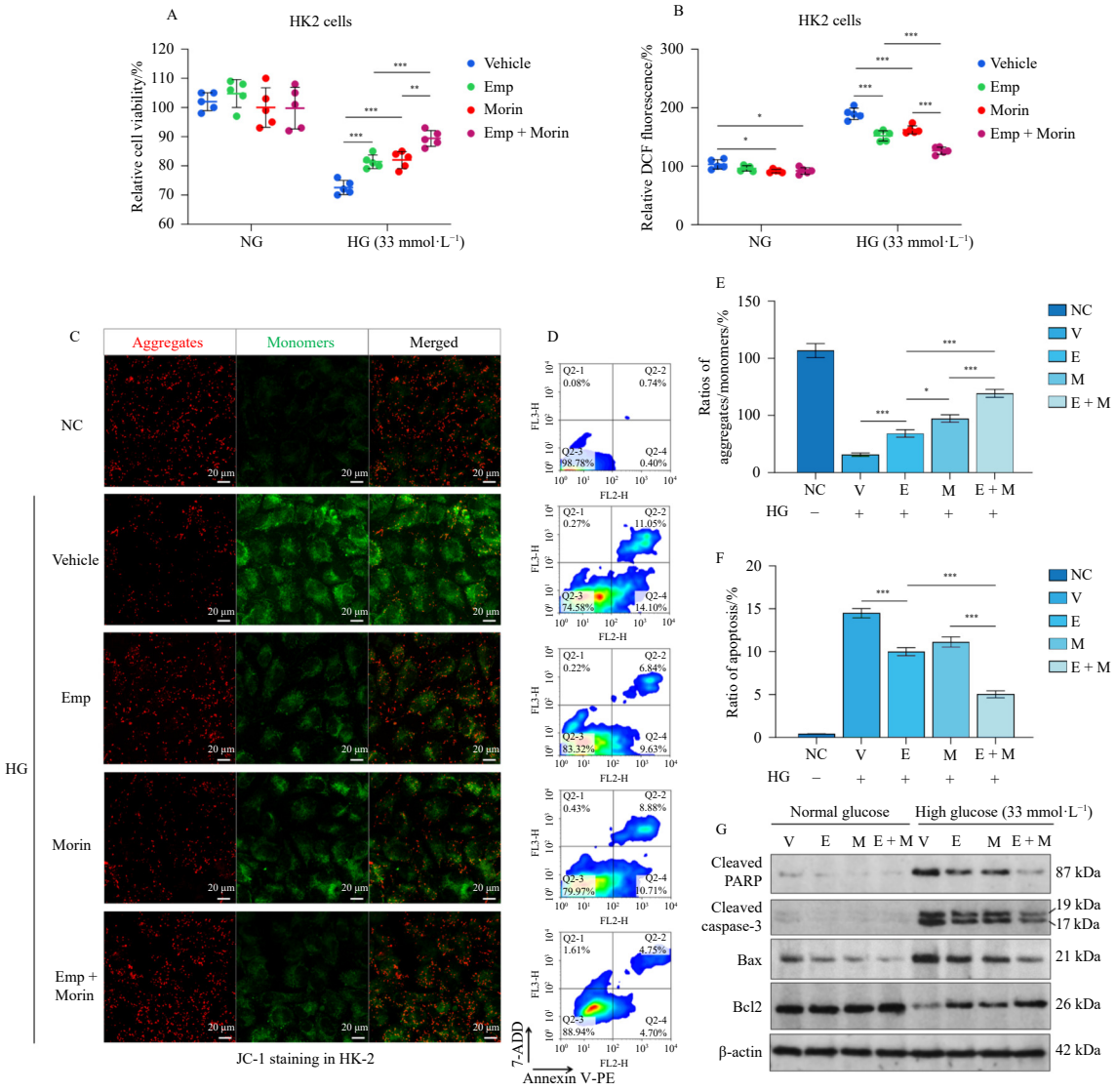

Fig. 1 Morin synergistically enhances the protective effects of Empagliflozin against high-glucose-induced intracellular ROS production and apoptosis in HK2 cells (A) Quantification of HK2 cell viability 48 h after treatment with culture medium with normal glucose (5.5 mmol·L^{-1}) (NG) or high-glucose (33 mmol·L^{-1}). In each subset, cells were treated with Empagliflozin (10 μmol·L^{-1}), Morin (50 μmol·L^{-1}) or their combination. (B) Quantification of intracellular reactive oxygen species (ROS) levels measured by DCFDA fluorescence. Cells were treated as indicated in panel A. (C and E) JC-1 staining in HK2 cells showing mitochondrial membrane potential changes. Red fluorescence indicates JC-1 aggregates (healthy mitochondria), while green fluorescence indicates JC-1 monomers (depolarized mitochondria). Cells were treated as indicated in panel A. Fluorescence ratio of JC-1 aggregates to monomers was quantified and compared in panel E. Scale bar: 20 μm. (D and F) Flow cytometry analysis of Annexin V-PE (FL2) and 7-AAD (FL3) staining to assess apoptosis in HK2 cells treated under the same conditions. Quadrants Q2-4, Q2-2 represent early and late apoptotic cells, respectively. Only early apoptotic cells were quantified in panel F. V: vehicle; E: Empagliflozin; M: Morin. (G) Western blot analysis of apoptotic markers (cleaved PARP, cleaved caspase-3), pro-apoptotic (Bax), and anti-apoptotic (Bcl2) proteins in HK2 cells as treated in panel A. n = 5 per group for panel A and B. n = 3 per group for panel E and F. One-way ANOVA followed by Tukey's post-hoc test was performed. $^{*}P$<0.05; $^{**}P$< 0.01; and $^{***}P$< 0.001 for indicated two-group comparison.

3.2. Morin protects against high-glucose-induced ER stress in proximal tubular cells

We next investigated the effects of Morin on ER stress in HK2 cells exposed to high-glucose conditions. High-glucose treatment markedly increased the expression of GRP78/BiP, p-PERK, p-eIF2α, CHOP, and cleaved ATF6 compared with the normal-glucose control (Figs. 2A, 2D, 2E, 2G, 2I, 2J). Treatment with Empagliflozin or Morin alone significantly reduced the levels of p-PERK, p-eIF2α, CHOP, and cleaved ATF6, whereas their combination resulted in a further decrease in these ER stress markers (Figs. 2E, 2G, 2I, 2J). GRP78/BiP expression was also attenuated by the combination treatment (Fig. 2D), whereas total PERK and eIF2α levels remained unchanged across groups (Figs. 2F, 2H).

Immunofluorescence staining demonstrated increased nuclear localization of ATF6 in HK2 cells under high-glucose conditions, as shown by the overlap of ATF6 (green) and nuclear (blue) signals in the merged images (Fig. 2B). Quantitative analysis of ATF6 MFI in the nucleus relative to total ATF6 confirmed a significant elevation in nuclear ATF6 following high-glucose exposure, which was partially reversed by Empagliflozin or Morin alone and further reduced by their combination (Fig. 2C). Collectively, these findings indicate that Morin effectively mitigates high-glucose-induced ER stress in proximal tubular cells and that combination treatment with Empagliflozin enhances this protective effect by modulating key ER stress markers and limiting ATF6 nuclear translocation.

3.3. Morin alleviates high-glucose-induced mitochondrial fission in proximal tubular cells

To investigate the effect of Morin on high-glucose-induced mitochondrial dynamics, we examined mitochondrial morphology using MitoTracker Green (Fig. 3A). High-glucose treatment induced significant mitochondrial fragmentation, as shown by the increased occurrence of punctate and fragmented mitochondrial

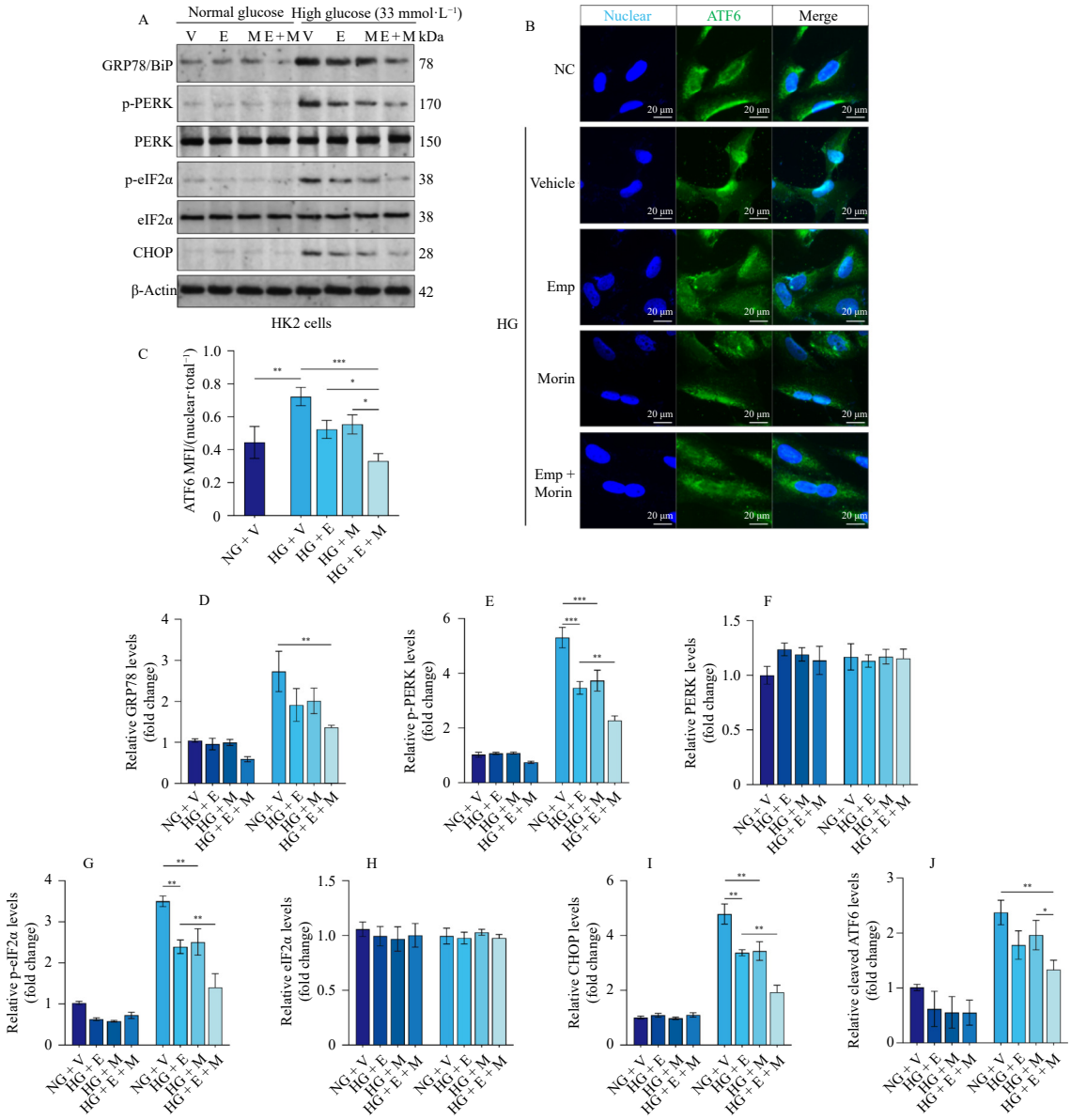

Fig. 2 Synergistic protection of Empagliflozin and Morin against high-glucose-induced ER stress (A) Western blot analysis of ER stress markers in HK2 cells. Cells were treated with normal glucose (NG, 5.5 mmol·L^{-1}), high glucose (HG, 33 mmol·L^{-1}), Empagliflozin (10 μmol·L^{-1}, E), Morin (50 μmol·L^{-1}, M), or a combination of Empagliflozin and Morin (E + M) for 48 h. The expression levels of GRP78/BiP, p-PERK, PERK, p-eIF2α, eIF2α, CHOP, ATF6, and cleaved ATF6 were analyzed. (B) Immunofluorescence staining of ATF6 in HK2 cells under the same treatment conditions as in (A). Representative images show the localization of nuclear (blue) and ATF6 (green). Scale bar: 20 μm. (C) Quantitative analysis of ATF6 nuclear translocation. Bar graph shows the ratio of nuclear ATF6 mean fluorescence intensity (MFI) to total ATF6. (D–J) Quantification of Western blot results from (A). Graphs depict the relative protein levels of (D) GRP78/BiP, (E) p-PERK, (F) PERK, (G) p-eIF2α, (H) eIF2α, (I) CHOP, and (J) cleaved ATF6 (n = 3). V: vehicle; E: Empagliflozin; M: Morin. Data are presented as fold change relative to NG control. One-way ANOVA followed by Tukey's post-hoc test was performed. Data are expressed as mean ± SD (n = 3). $^{*}P$<0.05; $^{**}P$< 0.01; and $^{***}P$< 0.001 for indicated two-group comparison.

structures (Fig. 4A, enhanced areas). Quantitative analysis revealed that the mitochondrial fission rate was significantly higher in the high-glucose group (Fig. 3B). Treatment with Empagliflozin or Morin alone moderately reduced the mitochondrial fission rate compared with the high-glucose group. The combination treatment with Empagliflozin and Morin demonstrated a synergistic effect (Fig. 3B).

Mitochondrial superoxide production was assessed using MitoSOX Red fluorescence. High-glucose conditions resulted in a marked increase in mitochondrial superoxide levels compared with normal glucose control. Treatment with Empagliflozin or Morin alone significantly reduced mitochondrial superoxide levels (Fig. 3C). Importantly, the combination treatment showed a synergistic effect, with a further reduction in mitochondrial superoxide production compared with each treatment alone (Fig. 3C).

Additionally, we analyzed the distribution of mitochondrial and cytosolic CytoC using immunofluorescence and Western blot assays (Figs. 3D–3E). In the high-glucose group, increased release of CytoC from mitochondria to the cytosol was observed, indicating mitochondrial stress. Empagliflozin and Morin individually reduced this release, and their combination provided a synergistic effect, maintaining more CytoC within the mitochondria and reducing its cytosolic presence (Figs. 3D–3E).

Next, we analyzed the expression levels of key mitochondrial fusion (Mfn1 and Mfn2) and fission (Fis1) proteins using Western blot (Fig. 3F). High-glucose treatment significantly decreased the expression of mitochondrial fusion proteins Mfn1 and Mfn2 whereas it increased the expression of the mitochondrial fission protein Fis1. Treatment with Empagliflozin or Morin alone partially restored Mfn1 and Mfn2 levels and reduced Fis1 levels. The combination treatment exhibited a synergistic enhancement, increasing Mfn1 and Mfn2 expression and decreasing Fis1 expression compared with each treatment alone

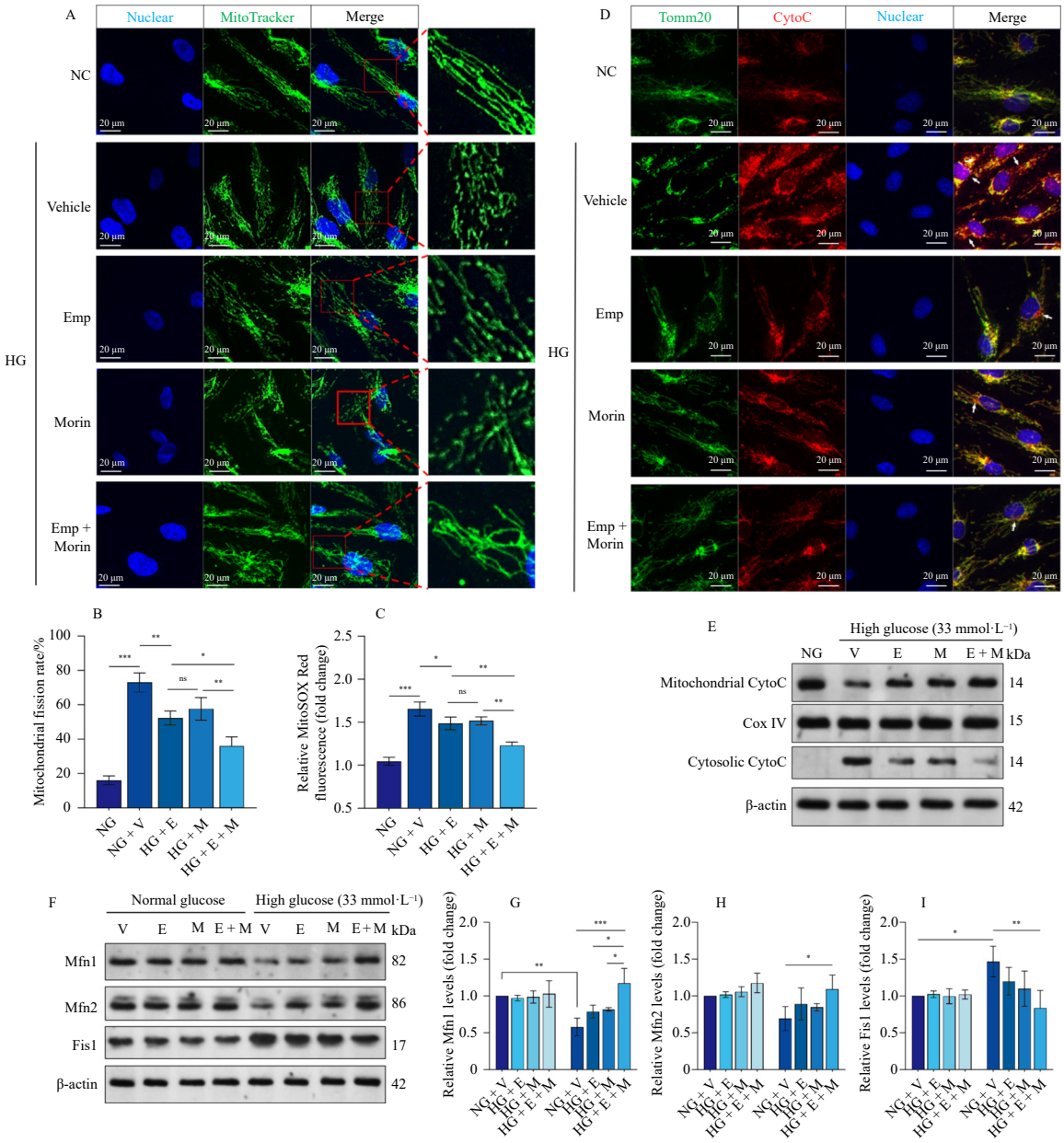

Fig. 3 Combined effect of Empagliflozin and Morin on high-glucose-induced mitochondrial fission (A) Representative immunofluorescence images showing mitochondrial morphology in HK2 cells treated with normal glucose (NG, 5.5 mmol·L^{-1}), high glucose (HG, 33 mmol·L^{-1}), Empagliflozin (10 μmol·L^{-1}), Morin (50 μmol·L^{-1}), or their combination for 48 h. Mitochondria were labeled with MitoTracker Green, and cell nuclei were marked with Hoechst 33342. Merged images highlight mitochondrial morphology. Scale bar: 20 μm. (B) Quantification of mitochondrial fission rate (%), defined by the equation: (fission events / total mitochondria) × 100, where the total mitochondria include fission, intermediate, and fusion types (n = 3). (C) Measurement of mitochondrial superoxide production using MitoSOX Red fluorescence intensity. Relative fold changes were calculated compared with the normal glucose control (n = 3). V: vehicle; E: Empagliflozin; M: Morin. (D) Representative immunofluorescence images showing mitochondrial and cytosolic cytochrome c (CytoC) in HK2 cells treated as in panel A. Mitochondria were labeled with Tomm20 (green), CytoC with red fluorescence, and nuclei with Hoechst 33342 (blue). Scale bar: 20 μm. (E) HK2 cells were treated with normal glucose (NG, 5.5 mmol·L^{-1}), high glucose (HG, 33 mmol·L^{-1}), Empagliflozin (10 μmol·L^{-1}, E), Morin (50 μmol·L^{-1}, M), or a combination of Empagliflozin and Morin (E + M) for 48 h. The expression of mitochondrial CytoC and cytosolic CytoC were checked. (F) Western blot analysis of mitochondrial fusion (Mfn1 and Mfn2) and fission (Fis1) proteins in HK2 cells treated as indicated in panel A. (G–I) Quantification of protein expression levels for Mfn1 (G), Mfn2 (H), and Fis1 (I) normalized to β-Actin (n = 3). V: vehicle; E: Empagliflozin; M: Morin. Data are presented as mean ± SD from three independent experiments. One-way ANOVA followed by Tukey's post-hoc test was performed. $^{*}P < 0.05$; $^{**}P < 0.01$; $^{***}P < 0.001$; ns, not significant for indicated two-group comparison.

(Figs. 3G–3I).

3.4. Bioinformatic analysis of the predicted targets of Empagliflozin and Morin

Having observed synergistic effects between Empagliflozin and Morin, we conducted bioinformatic analysis to explore the potential molecular mechanisms underlying their therapeutic effects. We first identified the predicted targets of these two compounds using SwissTargetPrediction (http://swisstargetprediction.ch/) [29]. The chemical structures of Empagliflozin (Fig. 4A top) and Morin (Fig. 4A bottom) were analyzed for target prediction (Supplementary Table 1). The Venn diagram showed that 13 targets were shared between the 101 predicted targets of Empagliflozin and the 104 predicted targets of Morin (Fig. 4C).

The top 25 predicted targets of Empagliflozin (Fig. 4B) were classified into various categories, including electrochemical transporter (24.0%), enzyme (16.0%), kinase (12.0%), and other functional groups. Similarly, the top predicted targets of Morin (Fig. 4D) encompassed enzyme (20.0%), family A/G protein-coupled receptor (16%), oxidoreductase (12.0%), primary active transporter (12%) nuclear receptor (12.0%), and several other categories.

To further characterize the functional relevance of these tar-

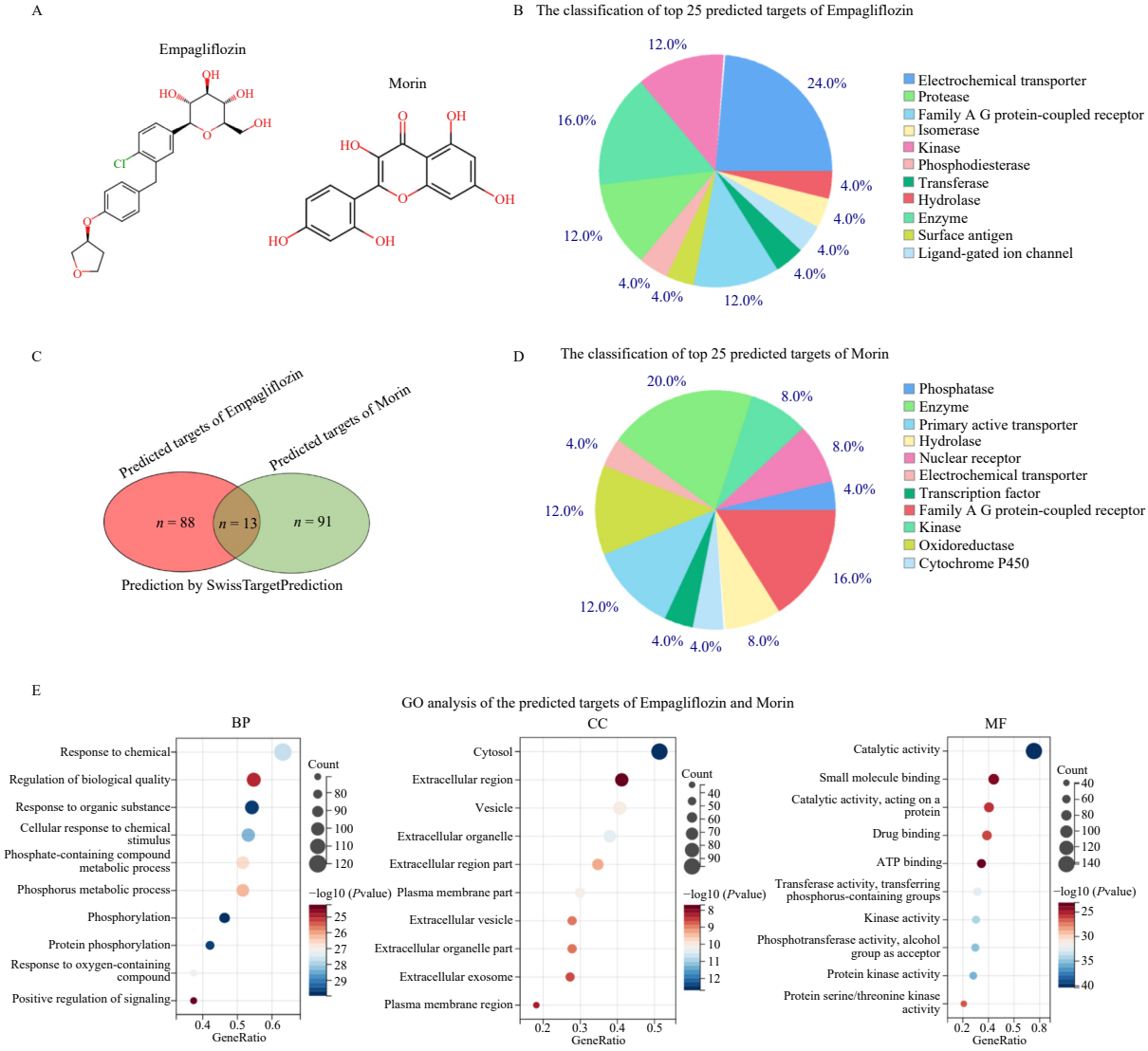

Fig. 4 Predicted targets of Empagliflozin and Morin of and gene ontology analysis (A) Chemical structure of Empagliflozin (top) and Morin (bottom). (B) Pie chart displaying the classification of the top 25 predicted targets of Empagliflozin. (C) Venn diagram showing the overlap in predicted targets between Empagliflozin and Morin. (D) Pie chart illustrating the classification of the top 25 predicted targets of Morin. (E) GO analysis of the predicted targets of Empagliflozin and Morin. The results are categorized into biological processes (left), cellular components (middle), and molecular functions (right), with each bubble representing specific GO terms. The size and color of the bubbles correspond to the gene ratio and -log10(*P*-value), respectively.

gets in biological processes (BPs), cellular components (CCs), and molecular functions (MFs), we performed Gene Ontology (GO) enrichment analysis using the full sets of predicted targets for both Empagliflozin and Morin (Supplementary Table 2). The GO analysis revealed that the predicted targets were enriched in several BPs, including response to chemical stimuli, regulation of biological quality, and phosphorylation (Fig. 4E, left). Regarding CCs, significant enrichments were observed in the cytosol, extracellular region, and plasma membrane compartments (Fig. 4E, middle). For MFs, the predicted targets were associated with catalytic activity, protein phosphorylation, and ATP binding (Fig. 4E, right). Of particular interest, many of these cellular locations are associated with key organelles involved in stress responses, such as the endoplasmic reticulum and mitochondria.

To identify specific targets of Morin in protecting HK2 cells from mitochondrial apoptosis, we examined the top candidates of Morin using SwissTargetPrediction (Fig. 5A). Among these, DAPK1 (Death-associated protein kinase 1) is a well-known regulator of apoptosis [22, 33, 34]. DAPK1 expression can be induced by activated ATF6 under ER stress conditions [19, 20]. Since Morin and Empagliflozin show inhibitory effects on ER stress signaling, including ATF6, we further explored their regulation on DAPK1 expression and activity. Although DAPK1 was not a predicted target of Empagliflozin, we selected DAPK1 as a key mechanistic focus in the combination treatment context because both Morin and Empagliflozin can regulate ATF6.

3.5. DAPK1 expression is regulated via ATF6 inhibition and its pro-apoptotic activity is inhibited through direct physical interaction

To clarify the mechanisms by which Morin and Empagliflozin regulate *DAPK1* expression, we generated ATF6-overexpression HK2 cells (Figs. 5B–5C). Under high-glucose conditions, which trigger ATF6 cleavage and nuclear translocation, *ATF6* overexpression led to a significant increase in *DAPK1* mRNA (Fig. 5D) and protein (Figs. 5E–5F) levels compared with vector controls, implying that activated ATF6 is a key transcriptional regulator of *DAPK1*. Both Morin and Empagliflozin significantly suppressed *DAPK1* expression in ATF6-OE cells under HG conditions, and their combination produced a synergistic effect (Figs. 5D–5F).

To directly test whether *ATF6* overexpression can reverse the inhibitory effects of Morin and Empagliflozin on *DAPK1* expression, we compared *DAPK1* mRNA levels in both vector control and ATF6-OE HK2 cells under high-glucose conditions with

A

Predicted target of Morin by SwissTargetPrediction

Target	Common name	Uniprot ID	Target Class	Probability
Receptor-type tyrosine-protein phosphatase S	PTPRS	Q13332	Phosphatase	0.34
Estrogen receptor beta	ESR2	Q92731	Nuclear receptor	0.34
Death-associated protein kinase 1	DAPK1	P53355	Kinase	0.34
DNA-3-methyladenine glycosylase	MPG	P29372	Enzyme	0.34
Solute carrier family 22 member 12	SLC22A12	Q96S37	Electrochemical transporter	0.34

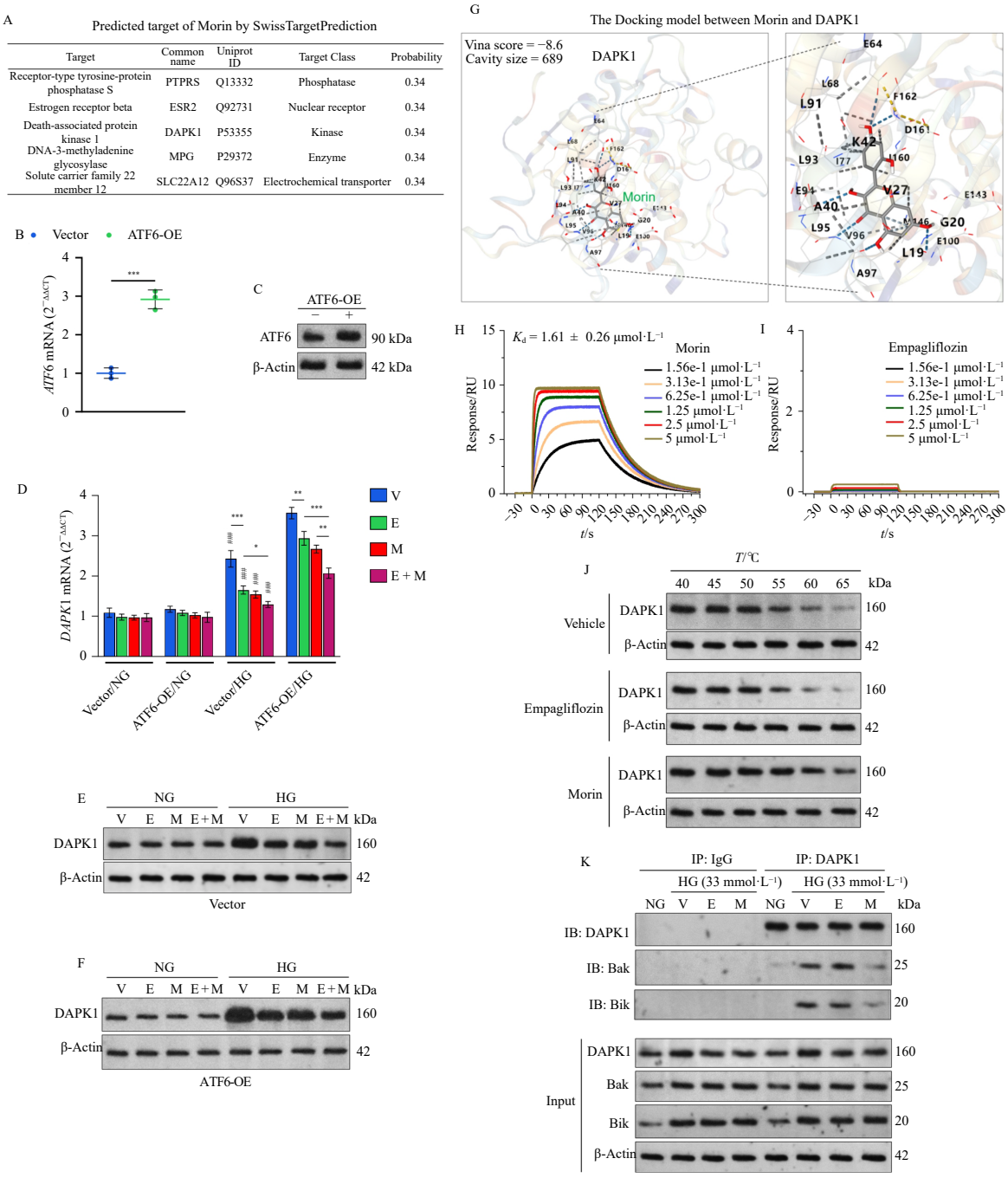

Fig. 5 Morin suppresses DAPK1 expression and inhibits its activity. (A) Predicted targets of Morin using SwissTargetPrediction, showing potential binding probabilities with various proteins, including DAPK1 (Death-associated protein kinase 1). (B–C) Relative mRNA (B) and protein (C) levels of ATF6 in HK2 cells with or without ATF6 overexpression. (D) Relative mRNA levels of *DAPK1* in HK2 cells under normal glucose (NG) or high glucose (HG, 33 mmol·L^{-1}) conditions for 48 h, with treatments of vehicle (V), Empagliflozin (E), Morin (M), or their combination (E + M), in both vector control and ATF6 overexpression groups. (E, F) Western blot analysis of DAPK1 protein levels in HK2 cells under NG or HG conditions, with indicated treatments, in vector control (E) and ATF6 overexpression (F) groups. (G) Molecular docking model illustrating the interaction between Morin and DAPK1, showing the predicted binding site and key interacting residues. (H) Sensorgram from surface plasmon resonance (SPR) analysis showing the binding kinetics of varying concentrations of Morin with DAPK1 and revealing a dissociation constant (*Kd*) of 1.61 ± 0.26 μmol·L^{-1}. (I) SPR analysis demonstrating that Empagliflozin does not show significant binding with DAPK1 at the tested concentrations. (J) Cellular lysates from HK2 cells treated with vehicle, Empagliflozin, or Morin were subjected to cellular thermal shift assay (CETSA) to detect DAPK1 stability under increasing temperature conditions (40–65 °C). (K) Co-immunoprecipitation (Co-IP) assay depicting the interaction between DAPK1 and pro-apoptotic proteins BAK and BIK under high glucose conditions (HG, 33 mmol·L^{-1}) with or without the presence of Empagliflozin (E) or Morin (M). DAPK1 was immunoprecipitated and the presence of BAK and BIK was detected by immunoblotting. Inputs were included for protein expression comparison. $^{*}P < 0.05$; $^{**}P < 0.01$; $^{\#\#\#}$and $^{***}P < 0.001$. $^{\#}$comparison between vector and ATF6-OE cells under the HG condition with the same treatment.

each treatment. Consistently, ATF6-OE cells exhibited significantly higher *DAPK1* expression under the same treatment (Morin and/or Empagliflozin) compared with vector control cells (Figs. 5D–5F). Notably, *ATF6* overexpression alone did not significantly increase *DAPK1* expression under normal glucose conditions (Figs. 5D–5F). This observation is consistent with the requirement for ATF6 proteolytic processing and nuclear translocation to function as an active transcription factor [19,35].

To investigate the potential direct interaction between Morin and DAPK1, we conducted a molecular docking analysis. The results illustrated a favorable binding affinity of Morin to DAPK1 (Vina score=-8.6) (Fig. 5G). This interaction was further confirmed by surface plasmon resonance (SPR) analysis, which showed that Morin bound to DAPK1 with a dissociation constant

(Kd) of 1.61 ± 0.26 μmol·L^{-1} (Fig. 5H). In contrast, SPR analysis indicated that Empagliflozin did not significantly bind to DAPK1 at the tested concentrations (Fig. 5I). Consistent with these findings, CETSA results showed that Morin, but not Empagliflozin, increased the thermal stability of DAPK1, further supporting a direct interaction between Morin and DAPK1 (Fig. 5J). This thermal stabilization arises because, when temperature exceeds a protein's intrinsic stability range, non-covalent interactions (hydrogen bonds, hydrophobic effects, salt bridges) that maintain the folded structure are disrupted, leading to unfolding (denaturation), exposure of hydrophobic residues, aggregation, and loss of solubility. Ligand binding can stabilize the folded structure, raising the melting temperature and rendering the protein more resistant to heat-induced denaturation. Importantly, this thermal stabilization is a biophysical characteristic measured under elevated temperatures and does not imply an increased protein half-life or abundance at physiological temperature (37 °C).

Although Empagliflozin did not directly bind to DAPK1, it still suppressed DAPK1 expression (Figs. 5D–5F). This indirect effect is likely mediated through inhibition of ER stress signaling, particularly ATF6 activation (Figs. 2A, 2I), which is known to transcriptionally upregulate DAPK1 under stress conditions [19, 20]. Thus, Empagliflozin reduces DAPK1 levels by modulating upstream signaling pathways rather than through direct protein interaction.

To further address the functional consequences of Morin binding, we examined whether Morin affects DAPK1 kinase activity and its interactions with pro-apoptotic partners. In the context of Bik-mediated apoptosis, DAPK1 is activated to form a complex with Bik, ERK1/2, and Bak, which is crucial for the induction of apoptotic processes [34]. Therefore, we further explored whether Morin affects the interaction between DAPK1 and the pro-apoptotic proteins BAK and BIK. Co-IP assays demonstrated that high glucose conditions enhance the interaction between DAPK1 and both BAK and BIK. Treatment with Morin significantly disrupted these interactions, whereas Empagliflozin had no comparable effect (Fig. 5K). Taken together, these results indicate that Morin inhibits DAPK1 function by both reducing its expression and interfering with its protein-protein interactions, rather than by destabilizing the protein itself.

3.6. Morin abrogates DAPK1 overexpression-induced excessive mitochondrial apoptosis under high-glucose condition

To further elucidate the protective role of Morin against DAPK1-induced mitochondrial apoptosis under high-glucose conditions, we assessed mitochondrial function and apoptosis in HK2 cells with *DAPK1* overexpression (Figs. 6A–6B). Western blot analysis revealed that cells with *DAPK1* overexpression exhibited significantly increased levels of cleaved PARP, cleaved caspase-3, and cytosolic CytoC after high-glucose treatment (Fig. 6C). Morin treatment markedly reduced these apoptotic markers, whereas Empagliflozin exerted weaker protective effects. The selective DAPK inhibitor TC-DAPK 6 (100 nmol·L^{-1}) effectively suppressed HG-induced apoptotic changes. Notably, TC-DAPK 6 showed no additive effect with Morin but displayed synergistic effects with Empagliflozin (Fig. 6D).

Flow cytometry analysis demonstrated that *DAPK1* overexpression significantly decreased mitochondrial membrane potential (TMRM fluorescence) and increased mitochondrial ROS production (MitoSOX Red fluorescence) under high-glucose conditions (Figs. 6E, 6G, 6I, 6K). Morin restored mitochondrial membrane potential and reduced mitochondrial ROS to levels comparable to TC-DAPK 6 treatment, while Empagliflozin produced partial protective effects (Figs. 6E–6L). In line with apoptosis marker results, TC-DAPK 6 did not enhance the effects of Morin but synergized with Empagliflozin (Figs. 6E–6L).

Annexin V/7-AAD staining revealed that high-glucose conditions induced a substantial increase in apoptosis in DAPK1-OE cells compared with vector control (Figs. 6M, 6N). Remarkably, Morin treatment significantly abrogated this increase in apoptosis, while Empagliflozin provided partial protection (Figs. 6M, 6N). Similar protective effects of Morin were observed when compared with TC-DAPK 6-treated cells (Figs. 6O, 6P). TC-DAPK 6 showed no additional protective effect when combined with Morin but demonstrated synergistic effects with Empagliflozin (Figs. 6O, 6P).

3.7. Synergistic renoprotection of Empagliflozin and Morin in a diabetic kidney disease model

To investigate the combined effects of Empagliflozin and Morin on high-glucose-induced diabetic kidney disease (DKD) *in vivo*, we used *db/db* mice as a model for type 2 diabetes. Five-week-old *db/m* and *db/db* mice were acclimatized and then subjected to different treatments for a period of 14 weeks. *db/m* mice were fed a normal diet, while *db/db* mice were fed a high-fat diet with the indicated treatments, including vehicle, Empagliflozin, low-dose Morin, high-dose Morin, or a combination of Empagliflozin and high-dose Morin (Fig. 7A). *db/db* mice treated with vehicle showed a progressive increase in body weight compared with *db/m* mice (Fig. 7B). Treatment with Empagliflozin, low Morin, high Morin, or their combination modulated weight gain in *db/db* mice, with the combination treatment group showing the most significant reduction in body weight compared with the vehicle-treated *db/db* group (Fig. 7B).

Kidney sections were stained with H&E, PAS, and Masson's trichrome to evaluate the morphology of renal tubular epithelial cells and the extent of renal fibrosis (Fig. 7C). Morphological analysis showed intact renal tubular epithelial cell structures with no noticeable pathological changes in the *db/m* group. In vehicle-treated *db/db* mice, H&E staining revealed epithelial cell shedding and tubular dilation, PAS staining showed increased glycoprotein deposition, and Masson's trichrome staining highlighted aggravated renal fibrosis. Compared with the vehicle group, renal tubular epithelial cell damage was alleviated by either Empagliflozin or Morin monotherapy, as evidenced by improved tubular structure, reduced glycoprotein deposition, and decreased fibrosis. The combination treatment with Empagliflozin and high-dose Morin demonstrated the most substantial protective effect, showing markedly reduced glomerulosclerosis and fibrosis, nearly restoring renal morphology to that observed in the healthy *db/m* group (Fig. 7C). Representative H&E images of colon sections are also shown, although no significant pathological changes were observed among groups.

To further validate the involvement of DAPK1 signaling and associated cell stress pathways *in vivo,* we examined protein expression of DAPK1, ER stress markers (GRP78, CHOP), and a mitochondrial apoptosis marker (cleaved caspase-3) in kidney tissues (Fig. 7D). Vehicle-treated *db/db* mice exhibited markedly elevated DAPK1, GRP78, CHOP, and cleaved caspase-3 compared with *db/m* mice, indicating activation of stress and apoptotic pathways. Both Empagliflozin and Morin monotherapies significantly reduced the expression of these proteins, whereas the combination treatment produced the most pronounced reduction, approaching the levels observed in healthy *db/m* controls. These findings support the conclusion that the synergistic renoprotective effect of Empagliflozin and Morin is at least partly mediated through suppression of DAPK1-related ER stress and mitochondrial apoptosis.

Blood glucose levels measured at different time points showed significant hyperglycemia in vehicle-treated *db/db* mice compared with *db/m* controls (Fig. 7E). Treatment with Empagliflozin or Morin alone significantly reduced blood glucose

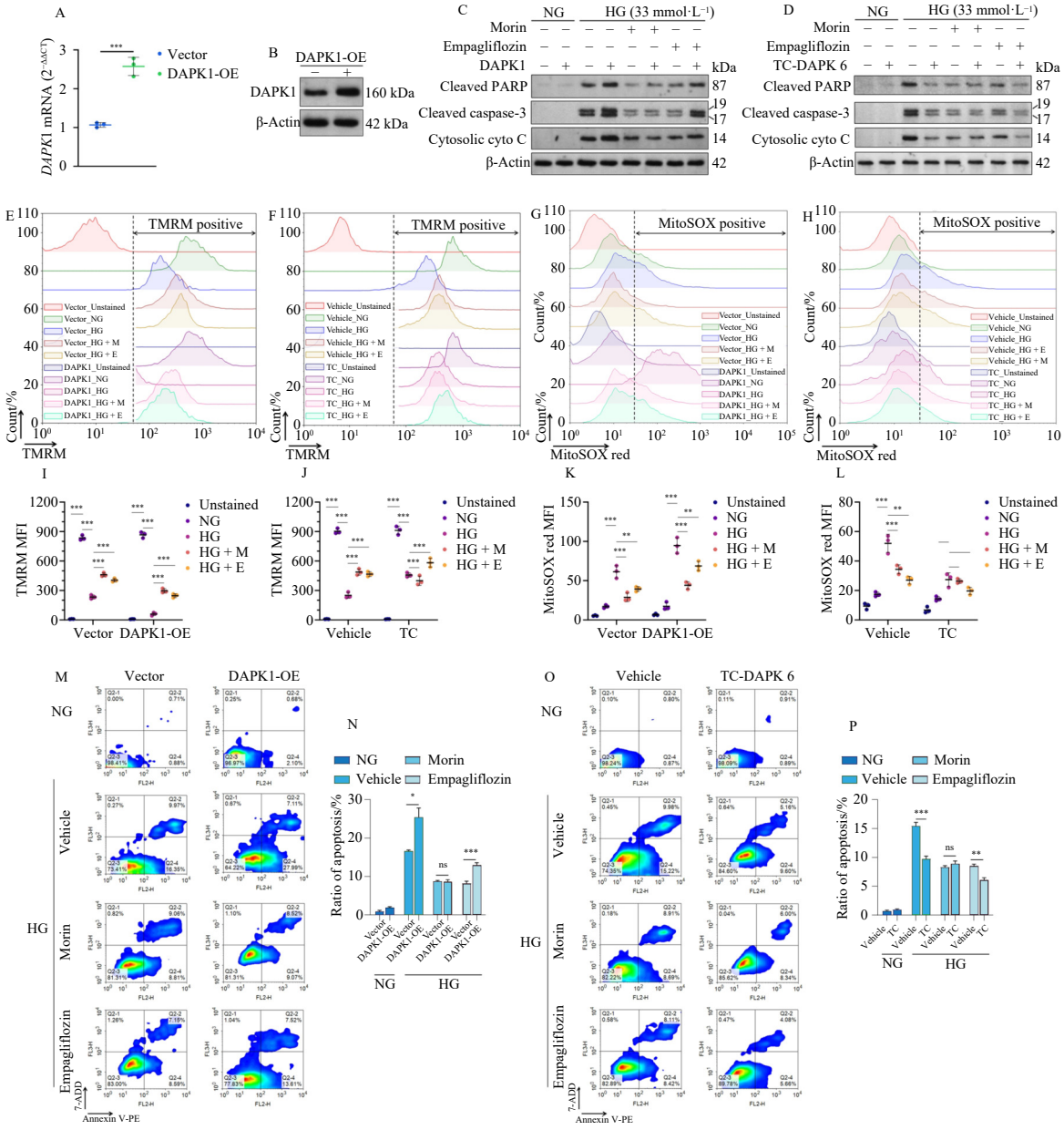

Fig. 6 Morin abrogates *DAPK1* overexpression-induced excessive mitochondrial apoptosis under high-glucose conditions (A–B) RT-qPCR (A, n=3) and Western blot (B) analyses showing the overexpression of DAPK1 in HK2 cells (DAPK1-OE) compared with vector control. (C–D) HK2 cells with or without *DAPK1* overexpression were treated with high glucose (HG, 33 mmol·L^{-1}) alone or with indicated Morin, Empagliflozin and/or TC-DAPK 6 (100 nmol·L^{-1}, a potent and highly selective DAPK inhibitor) treatment for 48 h. (E–F) Flow cytometry histograms showing TMRM fluorescence intensity (mitochondrial membrane potential) in vector and DAPK1-OE cells (E), and in vehicle and TC-DAPK6-treated cells (F) under the indicated treatments. (G–H) Flow cytometry histograms showing MitoSOX Red fluorescence intensity (mitochondrial ROS production) in vector and DAPK1-OE cells (G), and in vehicle and TC-DAPK 6-treated cells (H) under the indicated treatments. (I–L) Quantification of TMRM mean fluorescence intensity (MFI) (I–J) and MitoSOX Red MFI (K–L) in vector, DAPK1-OE, vehicle, and TC-DAPK 6 (TC) treated cells under the indicated treatments (n = 3). (M–O) Representative flow cytometry plots of Annexin V-PE and 7-AAD staining showing apoptotic cell populations in vector, DAPK1-OE (M), vehicle, and TC-DAPK 6 treated cells (O) under NG (normal glucose), HG (high-glucose, 33 mmol·L^{-1}), Morin, or Empagliflozin treatments. (N–P) Quantification of apoptotic cell ratios from panels M and O (n = 3). $^{*}P$<0.05, $^{***}P$ <0.001, ns = non-significant for indicated two-group comparison.

levels, and the combination treatment had a synergistic effect, resulting in the most profound reduction in blood glucose levels among the *db/db* groups (Fig. 7E). UACR was elevated in vehicle-treated *db/db* mice, indicating diabetic nephropathy (Fig. 7F). Treatment with Empagliflozin or Morin alone significantly reduced UACR, and the combination treatment resulted in a further reduction, highlighting the synergistic renoprotective effect of the combined therapy. Liver and kidney weights were recorded at the end of the experimental period (Figs. 7G–7H). Vehicle-treated *db/db* mice showed significantly increased liver weight compared with *db/m* mice (Fig. 7G). Treatment with Empagliflozin or Morin alone reduced liver weight, and the combination treatment led to the most significant reduction. Kidney weights did not show significant differences among the treatment groups (Fig. 7H).

4. Discussion

Previous studies have separately demonstrated the renoprotective effects of Empagliflozin or Morin in experimental models of diabetic kidney disease [13, 36, 37]. In this study, we demonstrated that the flavonoid Morin attenuated high-glucose-induced renal tubular cell injury by targeting DAPK1, a key regulator of mitochondrial apoptosis. Furthermore, combining Morin with Empagliflozin synergistically enhanced renal protection by suppressing both DAPK1 expression and activity. In animal models, the combination attenuated DKD progression in *db/db* mice and achieved better effects than either treatment alone. These find-

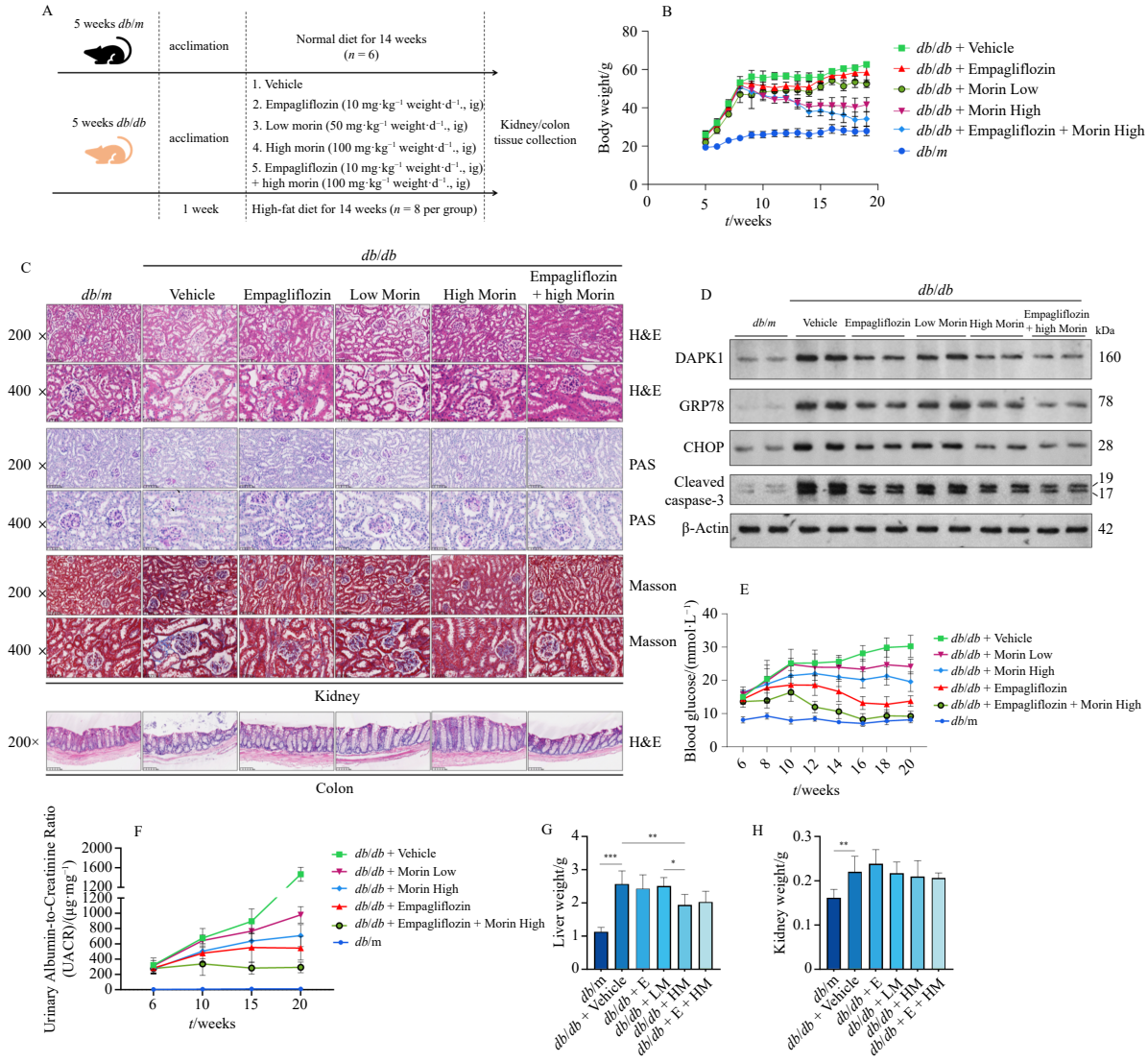

Fig. 7 Synergistic renoprotection of Empagliflozin and Morin in a diabetic kidney disease model. (A) Schematic diagram of experimental design. Five-week-old *db/m* and *db/db* mice were acclimated and then subjected to different treatments. *db/m* mice were fed a normal diet for 14 weeks ($n = 6$), while *db/db* mice were fed a high-fat diet for 14 weeks ($n = 8$ per group), with the following treatments: vehicle, Empagliflozin (10 mg·kg^{-1} weight/day), low Morin (50 mg·kg^{-1} weight/day), high Morin (100 mg·kg^{-1} weight/day), or a combination of Empagliflozin and high Morin. (B) Body weight measurements of mice over the experimental period. (C) Representative histological images of kidney sections stained with hematoxylin and eosin (H&E), periodic acid–Schiff (PAS), and Masson's trichrome. Images were taken at 200 × and 400 × magnifications. Additional images of colon sections stained with H&E are included. (D) Western blot analysis of kidney tissues from each treatment group, showing protein levels of DAPK1, GRP78, CHOP, and cleaved caspase-3. For each group, kidney samples from two mice were used for analysis. (E) Blood glucose levels measured at different time points throughout the experiment. (F) Urinary albumin-to-creatinine ratio (UACR) measurements at 6, 10, and 20 weeks. (G–H) Liver (G) and kidney (H) weight measurements at the end of the experimental period. Data represent mean ± SD. $^{*}P < 0.05$; $^{**}P < 0.01$; $^{***}P < 0.001$; ns, not significant.

ings highlight DAPK1 as a novel therapeutic target in DKD and provide mechanistic insights into the complementary actions of Morin and Empagliflozin.

ER stress is a critical factor in the pathogenesis of diabetic kidney disease, as it contributes to both renal cell apoptosis and fibrosis [4, 38]. Prolonged or unresolved ER stress can exacerbate cellular damage, leading to the activation of pro-apoptotic pathways and increased ROS production [3]. levated ROS production, from both mitochondrial and extracellular sources, further aggravates cellular dysfunction and damage [39]. ROS activate signaling pathways that disrupt mitochondrial function and promote mitochondrial fragmentation, a process tightly regulated by the balance between mitochondrial fission and fusion [40]. Under stress conditions such as hyperglycemia, mitochondrial fission is often excessive [41, 42].

DAPK1 promotes mitochondrial apoptosis by phosphorylating Bcl-2 family members, thereby triggering CytoC release and caspase activation [22]. In the context of Bik-mediated apoptosis, DAPK1 is required to form a complex with Bik, ERK1/2, and Bak [34]. Under ER stress, IFN-γ stimulates proteolytic processing of ATF6, which then forms a complex with C/EBP-β to induce *DAPK1* transcription, with both transcription factors being essential for *DAPK1* expression and autophagy induction [19-21]. Our findings extend these observations by demonstrating that *ATF6* overexpression significantly enhances *DAPK1* transcription under high-glucose conditions, while both Morin and Empagliflozin suppress this ATF6-mediated transcriptional activation. Furthermore, molecular docking, SPR, and CETSA assays confirmed a direct physical interaction between Morin and DAPK1, which reduces DAPK1's binding to pro-apoptotic partners BAK and BIK. This dual mechanism, transcriptional suppression and disruption of the kinase–protein complex, distinguishes Morin from conventional antioxidants and underscores its potential as a DAPK1-targeted therapy for DKD.

The *in vivo* results from our *db/db* mouse model further support the therapeutic potential of combining Empagliflozin and Morin for diabetic kidney disease. The synergistic effects were observed in several key parameters of diabetic nephropathy, by

reducing hyperglycemia, albuminuria (UACR), and renal fibrosis, compared with either treatment alone. The histological improvements-reduced glomerulosclerosis and glycoprotein deposition—mirror the *in vitro* attenuation of cellular stress, suggesting systemic benefits. Notably, the combination also mitigated hepatic steatosis (evidenced by reduced liver weight), a common comorbidity in diabetes, likely through Empagliflozin's metabolic effects and Morin's lipid-lowering properties. These findings support the concept of Morin as a viable adjunct to SGLT2 inhibition in DKD management.

However, some limitations should be acknowledged. First, although our *in vitro* experiments used a human proximal tubular cell line, it will be important to validate these findings in primary human renal cells to strengthen translational relevance. Second, although we confirmed that DAPK1 is a functionally important node targeted directly by Morin and indirectly by Empagliflozin, broader target profiling was not fully addressed. In our bioinformatic analysis, among the 13 predicted shared targets of the two compounds, the adenosine A2a receptor (ADORA2A) emerged as another candidate of interest (Supplementary Table 1). ADORA2A is known to modulate ER stress and mitochondrial function, with reported roles in enhancing mitochondrial metabolism, reducing ROS-mediated injury [43], and exerting anti-inflammatory effects via suppression of IL-1β and TNF-α production [44]. Future studies are warranted to determine whether ADORA2A constitutes an additional mechanistic link between Morin and Empagliflozin in the context of DKD. Furthermore, future work should aim to validate these findings in human-derived renal models (such as patient-derived organoids), expand mechanistic exploration to additional shared molecular targets, and evaluate long-term safety and efficacy in larger-scale and ultimately human studies. Such efforts would help accelerate the translation of Morin, in combination with SGLT2 inhibitors, toward clinical use for DKD management.

5. Conclusion

In summary, this study establishes DAPK1 as a critical mediator of hyperglycemia-induced renal tubular apoptosis and identifies Morin as a potent DAPK1 inhibitor. In addition, our study provides preclinical evidence for the synergistic protective effects of Empagliflozin and Morin against high-glucose-induced cellular stress and diabetic kidney disease. Given Empagliflozin's established therapeutic use and Morin's favorable safety profile as a natural compound, this combination merits further translational and clinical investigation as a promising adjunct strategy for DKD management.

Funding

This work was supported by the Natural Science Foundation of China (No. U22A20286).

Declaration of competing interests

These authors have no conflict of interest to declare.

Data Availability Statement

Data will be made available on reasonable request.

References

1 Li Y, Liu Y, Liu S, et al. Diabetic vascular diseases: molecular mechanisms and therapeutic strategies. *Signal Transduct Target Ther*. 2023;8(1):152. https://doi.org/10.1038/s41392-023-01400-z.
2 Nellaiappan K, Preeti K, Khatri DK, et al. Diabetic complications: an update on pathobiology and therapeutic strategies. *Curr Diabetes Rev*. 2022;18(1): e030821192146. https://doi.org/10.2174/1573399817666210309104203.
3 Liu Z, Nan P, Gong Y, et al. Endoplasmic reticulum stress-triggered ferroptosis *via* the XBP1-Hrd1-Nrf2 pathway induces EMT progression in diabetic nephropathy. *Biomed Pharmacother*. 2023;164:114897. https://doi.org/10.1016/j.biopha.2023.114897.
4 Li Q, Zhang K, Hou L, et al. Endoplasmic reticulum stress contributes to pyroptosis through NF-kappaB/NLRP3 pathway in diabetic nephropathy. *Life Sci*. 2023;322:121656. https://doi.org/10.1016/j.lfs.2023.121656.
5 Anker SD, Sander LE, Fitchett DH, et al. Empagliflozin in patients with type 2 diabetes mellitus and chronic obstructive pulmonary disease. *Diabetes Res Clin Pract*. 2022;186:109837. https://doi.org/10.1016/j.diabres.2022.109837.
6 Tsapas A, Avgerinos I, Karagiannis T, et al. Comparative effectiveness of glucose-lowering drugs for type 2 diabetes: a systematic review and network meta-analysis. *Ann Intern Med*. 2020;173(4):278-286. https://doi.org/10.7326/M20-0864.
7 Badreldin H, El-Karef A, Ibrahim T, et al. Targeting Nrf2/HO-1 and NF-kappaB/TNF-alpha signaling pathways with empagliflozin protects against atrial fibrillation-induced acute kidney injury in rats. *Toxicology*. 2024;506:153879. https://doi.org/10.1016/j.tox.2024.153879.
8 Sun X, Han F, Lu Q, et al. Empagliflozin ameliorates obesity-related cardiac dysfunction by regulating sestrin2-mediated AMPK-mTOR signaling and redox homeostasis in high-fat diet-induced obese mice. *Diabetes*. 2020;69(6):1292-1305. https://doi.org/10.2337/db19-0991.
9 Kapadia P, Bikkina P, Landicho MA, et al. Effect of anti-hyperglycemic drugs on endoplasmic reticulum (ER) stress in human coronary artery endothelial cells. *Eur J Pharmacol*. 2021;907:174249. https://doi.org/10.1016/j.ejphar.2021.174249.
10 Wu S, Luo X, Chen Y, et al. Sodium-glucose cotransporter 2 inhibitors attenuate vascular calcification by suppressing endoplasmic reticulum protein thioredoxin domain containing 5 dependent osteogenic reprogramming. *Redox Biol*. 2024;73:103183. https://doi.org/10.1016/j.redox.2024.103183.
11 V PV, Rajamanikandan S, Perumal MK. Morin inhibits the activity of pancreatic lipase and adipogenesis. *Eur J Pharmacol*. 2024;977:176705. https://doi.org/10.1016/j.ejphar.2024.176705.
12 Althagafy HS, Hassanein EHM. Morin mitigates 5-fluorouracil-induced nephrotoxicity by activating Nrf2/HO-1 and FXR, and suppressing ERK/VCAM-1 and NF-kappaB pathways. *Int Immunopharmacol*. 2025;148:114092. https://doi.org/10.1016/j.intimp.2025.114092.
13 Hua Z, Li Y, Chen T, et al. Morin-based nanoparticles for regulation of blood glucose. *ACS Appl Mater Interfaces*. 2024;16(17):21400-21414. https://doi.org/10.1021/acsami.3c17642.
14 Rajput SA, Wang XQ, Yan HC. Morin hydrate: a comprehensive review on novel natural dietary bioactive compound with versatile biological and pharmacological potential. *Biomed Pharmacother*. 2021;138:111511. https://doi.org/10.1016/j.biopha.2021.111511.
15 Tian Y, Li Z, Shen B, et al. Protective effects of morin on lipopolysaccharide/*d*-galactosamine-induced acute liver injury by inhibiting TLR4/NF-kappaB and activating Nrf2/HO-1 signaling pathways. *Int Immunopharmacol*. 2017;45:148-155. https://doi.org/10.1016/j.intimp.2017.02.010.
16 Jiang A, Zhang Y, Zhang X, et al. Morin alleviates LPS-induced mastitis by inhibiting the PI3K/AKT, MAPK, NF-kappaB and NLRP3 signaling pathway and protecting the integrity of blood-milk barrier. *Int Immunopharmacol*. 2020;78:105972. https://doi.org/10.1016/j.intimp.2019.105972.
17 Singh MP, Chauhan AK, Kang SC. Morin hydrate ameliorates cisplatin-induced ER stress, inflammation and autophagy in HEK-293 cells and mice kidney *via* PARP-1 regulation. *Int Immunopharmacol*. 2018;56:156-167. https://doi.org/10.1016/j.intimp.2018.01.031.
18 Kumar Pandey V, Mathur A, Fareed Khan M, et al. Endoplasmic reticulum stress induces degradation of glucose transporter proteins during hyperglycemic hepatotoxicity: role of PERK-eIF2alpha-ATF4 axis. *Eur J Pharmacol*. 2022;926:175012. https://doi.org/10.1016/j.ejphar.2022.175012.
19 Gade P, Ramachandran G, Maachani UB, et al. An IFN-gamma-stimulated ATF6-C/EBP-beta-signaling pathway critical for the expression of death associated protein kinase 1 and induction of autophagy. *Proc Natl Acad Sci U S A*. 2012;109(26):10316-10321. https://doi.org/10.1073/pnas.1119273109.
20 Zhou Y, Zhang S, Dai C, et al. Quinocetone triggered ER stress-induced autophagy *via* ATF6/DAPK1-modulated mAtg9a trafficking. *Cell Biol Toxicol*. 2016;32(2):141-152. https://doi.org/10.1007/s10565-016-9323-3.
21 Lopes F, Keita AV, Saxena A, et al. ER-stress mobilization of death-associated protein kinase-1-dependent xenophagy counteracts mitochondria stress-induced epithelial barrier dysfunction. *J Biol Chem*. 2018;293(9):3073-3087. https://doi.org/10.1074/jbc.RA117.000809.
22 Wang Y, Fang X, Yang Y, et al. Death-associated protein kinase 1 promotes alveolar epithelial cell apoptosis and ventilator-induced lung injury through p53 pathway. *Shock*. 2022;57(1):140-150. https://doi.org/10.1097/SHK.0000000000001831.
23 Wu GJ, Zhao HB, Zhang XW. Death-associated protein kinase 1 correlates with podocyte apoptosis and renal damage and can be mediated by miR-361. *Histol Histopathol*. 2021;36(11):1155-1167. https://doi.org/10.14670/HH-18-358.
24 Zafari F, Shirian S, Sadeghi M, et al. CD93 hematopoietic stem cells improve diabetic wound healing by VEGF activation and downregulation of DAPK-1. *J Cell Physiol*. 2020;235(3):2366-2376. https://doi.org/10.1002/jcp.29142.
25 Paoli P, Cirri P, Caselli A, et al. The insulin-mimetic effect of morin: a promising molecule in diabetes treatment. *Biochim Biophys Acta*. 2013;1830(4):3102-3111. https://doi.org/10.1016/j.bbagen.2013.01.017.
26 Steven S, Oelze M, Hanf A, et al. The SGLT2 inhibitor empagliflozin improves the primary diabetic complications in ZDF rats. *Redox Biol*. 2017;13:370-385.

https://doi.org/10.1016/j.redox.2017.06.009.
27 Okamoto M, Takayama K, Shimizu T, et al. Identification of death-associated protein kinases inhibitors using structure-based virtual screening. *J Med Chem*. 2009;52(22):7323-7327. https://doi.org/10.1021/jm901191q.
28 Zhou D, Zhong S, Han X, et al. Protocol for mitochondrial isolation and subcellular localization assay for mitochondrial proteins. *STAR Protoc*. 2023;4 (1):102088. https://doi.org/10.1016/j.xpro.2023.102088.
29 Daina A, Michielin O, Zoete V. SwissTargetPrediction: updated data and new features for efficient prediction of protein targets of small molecules. *Nucleic Acids Res*. 2019;47(W1):W357-W364. https://doi.org/10.1093/nar/gkz382.
30 Liu Y, Grimm M, Dai WT, et al. CB-Dock: a web server for cavity detection-guided protein-ligand blind docking. *Acta Pharmacol Sin*. 2020;41(1):138-144. https://doi.org/10.1038/s41401-019-0228-6.
31 Yokoyama T, Kusaka K. Characterization of the molecular interactions between resveratrol derivatives and death-associated protein kinase 1. *FEBS J*. 2023;290(18):4465-4479. https://doi.org/10.1111/febs.16817.
32 Han JX, Luo LL, Wang YC, et al. SGLT2 inhibitor empagliflozin promotes revascularization in diabetic mouse hindlimb ischemia by inhibiting ferroptosis. *Acta Pharmacol Sin*. 2023;44(6):1161-1174. https://doi.org/10.1038/s41401-022-01031-0.
33 Pei L, Shang Y, Jin H, et al. DAPK1-p53 interaction converges necrotic and apoptotic pathways of ischemic neuronal death. *J Neurosci*. 2014;34(19): 6546-6556. https://doi.org/10.1523/JNEUROSCI.5119-13.2014.
34 Mebratu YA, Leyva-Baca I, Wathelet MG, et al. Bik reduces hyperplastic cells by increasing Bak and activating DAPk1 to juxtapose ER and mitochondria. *Nat Commun*. 2017;8(1):803. https://doi.org/10.1038/s41467-017-00975-w.
35 Haze K, Yoshida H, Yanagi H, et al. Mammalian transcription factor ATF6 is synthesized as a transmembrane protein and activated by proteolysis in response to endoplasmic reticulum stress. *Mol Biol Cell*. 1999;10(11):3787-3799. https://doi.org/10.1091/mbc.10.11.3787.
36 Pirklbauer M, Sallaberger S, Staudinger P, et al. Empagliflozin inhibits IL-1beta-mediated inflammatory response in human proximal tubular cells. *Int J Mol Sci*. 2021;22(10):5089. https://doi.org/10.3390/ijms22105089.
37 Matsui S, Yamamoto T, Takabatake Y, et al. Empagliflozin protects the kidney by reducing toxic ALB (albumin) exposure and preventing autophagic stagnation in proximal tubules. *Autophagy*. 2024:1-15. doi:10.1080/15548627.2024.2410621
38 Wu X, Li H, Wan Z, et al. The combination of ursolic acid and empagliflozin relieves diabetic nephropathy by reducing inflammation, oxidative stress and renal fibrosis. *Biomed Pharmacother*. 2021;144:112267. https://doi.org/10.1016/j.biopha.2021.112267.
39 Yang J, Liu Z. Mechanistic pathogenesis of endothelial dysfunction in diabetic nephropathy and retinopathy. *Front Endocrinol (Lausanne)*. 2022;13:816400. https://doi.org/10.3389/fendo.2022.816400.
40 Liu BH, Xu CZ, Liu Y, et al. Mitochondrial quality control in human health and disease. *Mil Med Res*. 2024;11(1):32. https://doi.org/10.1186/s40779-024-00536-5.
41 Wang T, Wang X, Fu T, et al. Roles of mitochondrial dynamics and mitophagy in diabetic myocardial microvascular injury. *Cell Stress Chaperones*. 2023;28 (6):675-688. https://doi.org/10.1007/s12192-023-01384-3.
42 Ma F, Li H, Huo H, et al. N-acetyl-L-cysteine alleviates FUNDC1-mediated mitophagy by regulating mitochondrial dynamics in type 1 diabetic nephropathy canine. *Life Sci*. 2023;313:121278. https://doi.org/10.1016/j.lfs.2022.121278.
43 Castro CM, Corciulo C, Solesio ME, et al. Adenosine A2A receptor (A2AR) stimulation enhances mitochondrial metabolism and mitigates reactive oxygen species-mediated mitochondrial injury. *FASEB J*. 2020;34(4):5027-5045. https://doi.org/10.1096/fj.201902459R.
44 Fu SY, Xiong RP, Peng Y, et al. PKC mediates LPS-induced IL-1beta expression and participates in the pro-inflammatory effect of A(2A)R under high glutamate concentrations in mouse microglia. *Neurochem Res*. 2019;44 (12):2755-2764. https://doi.org/10.1007/s11064-019-02895-1.